Organic & Biomolecular Chemistry

Cite this: *Org. Biomol. Chem.*, 2011, **9**, 4936

www.rsc.org/obc

PAPER

Oxidation of 4-substituted TEMPO derivatives reveals modifications at the 1- and 4-positions†‡

David L. Marshall,[a] Meganne L. Christian,[b] Ganna Gryn'ova,[c] Michelle L. Coote,[c] Philip J. Barker[a,b] and Stephen J. Blanksby*[a]

Received 7th January 2011, Accepted 7th April 2011
DOI: 10.1039/c1ob05037k

Potenital pathways for the deactivation of hindered amine light stabilisers (HALS) have been investigated by observing reactions of model compounds—based on 4-substituted derivatives of 2,2,6,6-tetramethylpiperidine-*N*-oxyl (TEMPO)—with hydroxyl radicals. In these reactions, dilute aqueous suspensions of photocatalytic nanoparticulate titanium dioxide were irradiated with UV light in the presence of water-soluble TEMPO derivatives. Electron spin resonance (ESR) and electrospray ionisation mass-spectrometry (ESI-MS) data were acquired to provide complementary structural elucidation of the odd- and even-electron products of these reactions and both techniques show evidence for the formation of 4-oxo-TEMPO (TEMPONE). TEMPONE formation from the 4-substituted TEMPO compounds is proposed to be initiated by hydrogen abstraction at the 4-position by hydroxyl radical. High-level *ab initio* calculations reveal a thermodynamic preference for abstraction of this hydrogen but computed activation barriers indicate that, although viable, it is less favoured than hydrogen abstraction from elsewhere on the TEMPO scaffold. If a radical is formed at the 4-position however, calculations elucidate two reaction pathways leading to TEMPONE following combination with either a second hydroxyl radical or dioxygen. An alternate mechanism for conversion of TEMPOL to TEMPONE *via* an alkoxyl radical intermediate is also considered and found to be competitive with the other pathways. ESI-MS analysis also shows an increased abundance of analogous 4-substituted piperidines during the course of irradiation, suggesting competitive modification at the 1-position to produce a secondary amine. This modification is confirmed by characteristic fragmentation patterns of the ionised piperidines obtained by tandem mass spectrometry. The conclusions describe how reaction at the 4-position could be responsible for the gradual depletion of HALS in pigmented surface coatings and secondly, that modification at nitrogen to form the corresponding secondary amine species may play a greater role in the stabilisation mechanisms of HALS than previously considered.

Introduction

Nitroxyl radicals based on 2,2,6,6-tetramethylpiperidinyl-*N*-oxyl (TEMPO) are highly stable, isolable species.[1] The addition of TEMPO to alkyl and acyl radicals occurs below the diffusion-controlled limit, but nonetheless these trapping reactions proceed more readily than dimerisation or other self-reactions of TEMPO.[2] A variety of TEMPO derivatives are therefore used as spin labels for supramolecular complexes;[3] reversible inhibitors for nitroxide mediated polymerisation;[4] and as superoxide dismutase mimetics for the protection of biomolecules against oxidative stress.[5] Similarly, derivatives of TEMPO can act as radical scavenging, anti-oxidant stabilisers for polymers, improving durability and aesthetic properties throughout their service lifetime. By using a colourless precursor to generate the TEMPO-based nitroxyl *in situ*, hindered amine light stabilisers (HALS) are widely used to prolong the lifetime of automotive coatings, bulk polymers, and thin films.[6]

[a]*ARC Centre of Excellence for Free Radical Chemistry and Biotechnology, School of Chemistry, University of Wollongong, Northfields Ave, Wollongong, NSW 2522, Australia. E-mail: blanksby@uow.edu.au; Fax: +61 2 4221 4287; Tel: +61 2 4221 5484*

[b]*BlueScope Steel Research, PO Box 202, Port Kembla, NSW 2505, Australia*

[c]*ARC Centre of Excellence for Free Radical Chemistry and Biotechnology, Research School of Chemistry, Australian National University, Canberra, ACT 0200, Australia*

† This work is dedicated to the memory of Athel Beckwith. Two of us (P.J. Barker and M.L. Coote) have first hand experience of his mentorship as co-workers, while all of us have benefited from his many and varied contributions to free-radical chemistry.

‡ Electronic supplementary information (ESI) available: ESI-MS spectra for the irradiation of **3** and **4**, analogous to Fig. 5. Normalised energy profiles for TEMPONE formation from each of **2**–**4** (see Schemes 4 and 5). Optimised geometries in the form of GAUSSIAN archive entries, corresponding total energies, thermal corrections, zero-point vibrational energies, entropies, free energies and free energies of solvation. See DOI: 10.1039/c1ob05037k

The predominant mode of HALS action is believed to involve activation of the 2,2,6,6-tetramethylpiperidine moiety (TEMP-X, X = H, alkyl, or ether, Scheme 1) to the equivalent TEMPO free radical, which subsequently scavenges otherwise reactive polymeric alkyl or acyl radicals to form an amino-ether (TEMPO-R).[7] Upon further reaction with a peroxyl radical, the nitroxyl radical is regenerated, converting harmful propagating radical species to less reactive even-electron by-products, as in Scheme 1.

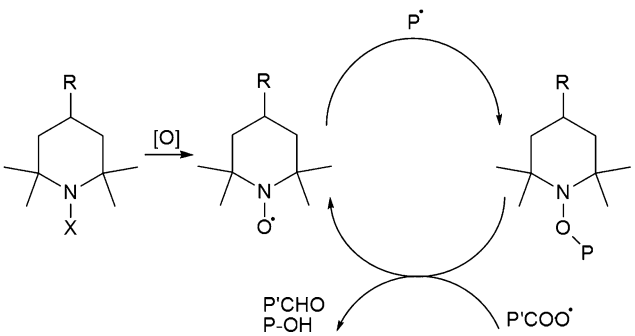

Scheme 1 A generalised stabilisation mechanism for HALS.

The exact nature of the oxidation and propagation processes described by Scheme 1 remains an area of active discussion,[8] however, little is known about the fate of active HALS molecules in-service. Testing HALS molecules for efficacy in surface coatings involves empirically monitoring aesthetic properties in HALS-doped coatings to demonstrate an extension of product lifetime in a specific application, compared to a control coating.[9] Such investigations demonstrate that the benefits afforded by HALS are finite, as shown by the eventual discolouring, fading, or degradation of the stabilised polymer, with the gradual decline in physical properties mirrored by a concomitant decrease in the concentration of available active HALS within the polymer over time.[10] Current understanding is limited as to why HALS do not stabilise polymers catalytically and indefinitely, as might be expected from Scheme 1. Characterisation of deactivation mechanisms could be crucial in selecting appropriate HALS for specific applications.

In principle, there are several general mechanisms by which HALS molecules could be deactivated or decomposed. HALS have been shown to migrate into lower coating layers where they can no longer act as efficient stabilisers.[11] Deactivation driven by the inherent basicity of HALS could occur by chemisorption onto activated particle surfaces within the polymeric matrix, particularly in highly pigmented coatings,[12] or by acid/base interactions with the catalysts of acid-curing surface coatings. Chemical or photochemical decomposition of HALS can lead to the formation of non-oxidisable adducts whereby regeneration of the active nitroxyl is inhibited.[13] Moreover, the deactivation of HALS need not depend on the modification of the nitroxyl radical. Oxidative decomposition can cause HALS fragments to be volatilised from the coating during high temperature processing or in-service. Low molecular weight methoxy- and hydroxy-piperidines were detected when ester-linked oligomeric HALS in polypropylene were subjected to ultraviolet (UV) light.[14] Similarly, after prolonged ambient exposure of polyethylene films, 4-amino-2,2,6,6-tetramethylpiperidine was detected as a decomposition product of HALS possessing a secondary amine linkage at the 4-position (R^4).[15]

In order to complement such studies, simplified chemical systems are employed in mechanistic studies of antioxidant action to elucidate plausible reaction pathways. For example, simple derivatives of TEMPO have been employed as putative models for studying chemical reactions at the active sites of HALS.[7c] Further studies, undertaken from a medicinal perspective, reported that 4-hydroxy-TEMPO (TEMPOL) is susceptible to modification at the 4-position, leading to the formation of 4-oxo-TEMPO (TEMPONE), proposed to occur *via* the mechanism shown in Scheme 2. In many currently utilised HALS, the active TEMPO moiety is anchored to a larger molecular weight scaffold at R^4, and thus such an elimination could lead to deactivation of HALS *via* volatilisation of the low mass TEMPONE fragment.

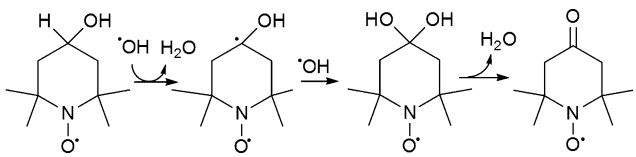

Scheme 2 Proposed mechanism for the hydroxyl radical induced formation of 4-oxo-TEMPO (TEMPONE) from 4-hydroxy-TEMPO (TEMPOL).[16]

In this study we have undertaken a detailed experimental and theoretical investigation of the reactions of TEMPO and selected 4-substituted TEMPO derivatives (**1–5**, Fig. 1) with hydroxyl radicals (HO•), with an aim to identify pathways that might lead to deactivation of these compounds, and thus by extension deactivation of HALS in polymer coatings. Hydroxyl radicals were generated by irradiating dilute aqueous suspensions of AEROXIDE® P-25 nanoparticulate titanium dioxide, providing a milder approach than direct photolysis or radiolysis of hydrogen peroxide solutions. The conditions also allow a greater opportunity to observe the evolution of the reaction (and potential reaction intermediates) by both electron spin resonance (ESR) spectroscopy and electrospray ionisation mass spectrometry (ESI-MS), in contrast to traditional end-product analysis. Moreover, this method is of direct relevance to the conditions

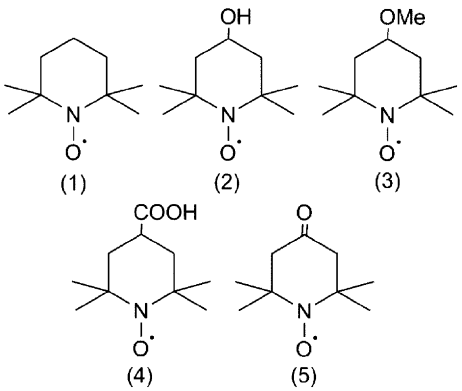

Fig. 1 TEMPO derivatives used as HALS model compounds: (**1**) 2,2,6,6-tetramethylpiperidine-*N*-oxyl 'TEMPO'; (**2**) 4-hydroxy-2,2,6,6-tetramethylpiperidine-*N*-oxyl 'TEMPOL'; (**3**) 4-methoxy-2,2,6,6-tetramethylpiperidine-*N*-oxyl '4-methoxy-TEMPO'; (**4**) 4-carboxy-2,2,6,6-tetramethylpiperidine-*N*-oxyl '4-carboxy-TEMPO'; (**5**) 4-oxo-2,2,6,6-tetramethylpiperidine-*N*-oxyl 'TEMPONE'.

encountered by HALS *in situ*, as titanium dioxide is a common inorganic pigment present in polymer coatings. Both pigmentary and nanoparticulate grades of titanium dioxide accelerate the degradation of polymer films, with little benefit afforded by HALS due to their photocatalytic destruction.[17] Perhaps the most astonishing demonstration of the photocatalytic destruction of durable surface coatings containing HALS is that caused by certain commercial sunscreen formulations, in which the presence of photocatalytic grades of titanium dioxide were confirmed spectroscopically.[18] While not quantitative in nature, this combined experimental and theoretical study identifies potential mechanisms of TEMPO degradation and deactivation that are not accounted for by current descriptions of their major reactivity pathways (*cf*. Scheme 1). The identification of thoroughly characterised mechanisms for irreversible chemical deactivation of TEMPO derivatives, even if minor compared to well-established nitroxyl radical chemistry, provides important new understanding of long term HALS deactivation over the service lifetime of surface coatings.

Experimental

Materials

TEMPO derivatives and the corresponding piperidine analogues were purchased from Sigma Aldrich (Castle Hill, Australia), stored at 4 °C, and used without further purification. AEROXIDE® P-25 TiO_2 was a gift from Evonik (Essen, Germany). Deionised water (reverse osmosis, median conductivity $3–4 \times 10^{-6}$ S m^{-1}) was employed throughout. Solvents employed for mass spectrometry (acetonitrile and methanol) were HPLC grade (Ajax Finechem, Taren Point, Australia) and used as received. Solvents used for thin layer chromatographic (TLC) analysis (ethyl acetate, hexane and triethylamine) were reagent grade (Ajax Finechem, Australia) and also used as received.

Photochemistry

Photolysis experiments were carried out in a custom-built reactor, with a 1 kW Xe arc lamp (Oriel Corporation, Stratford, CT, USA) producing a collimated parallel beam of 4.8 cm diameter. The system was equipped with a 10 cm pathlength infrared filter (water), a green glass filter passing only wavelengths above 375 nm, and a neutral density attenuation filter passing 30% of the incident light. The filtered beam entered a quartz reactor, containing a stirring suspension of P-25 TiO_2 (125 mg) and the TEMPO derivative **1–5** (100 μM) in 200 cm^3 water. The reactor was enclosed within a dark box, fitted with an extractor fan for temperature control, and openings for sampling and stirrer control. Samples (*ca.* 1.5 cm^3) were taken at regular time intervals, centrifuged, and the supernatant transferred to a quartz ESR flat cell (active volume 0.15 cm^3). After the ESR measurement, the solutions were reserved for mass spectrometric analysis. Control experiments were undertaken whereby TEMPO solutions were mixed with TiO_2 maintained in darkness, and irradiated under identical experimental conditions for 3 h in the absence of TiO_2.

ESR spectroscopy

ESR data was obtained on a Bruker ESP300E spectrometer (Bruker GmbH, Rheinstetten, Germany) operating in the X-band of the microwave spectrum, equipped with an NMR gaussmeter and frequency counter. Instrument settings were as follows: microwave power, 2.0 mW; modulation frequency, 100 kHz; modulation amplitude, 0.2 mT. Measurements were conducted in a climate-controlled laboratory at 20.0 °C ± 0.5 °C. For the solution mixing experiments, 5 cm^3 of a 100 μM TEMPOL solution was placed in a small vial. A similar solution of TEMPONE was added dropwise, with ESR spectra recorded after the addition of every drop until the relative concentrations were in the range similar to those observed in the photolysis experiments. The composite spectra were scaled to a similar intensity to the experimental spectra.

Mass spectrometry and chromatography

Positive ion mass spectra were recorded with a Waters QuattroMicro (Waters, Manchester, U.K.) triple quadrupole mass spectrometer equipped with an ESI source and controlled by Micromass MassLynx software (version 4.1). The aqueous solutions were diluted to *ca.* 15 μM in acetonitrile, and infused directly into the ESI source at 10 μL min^{-1}. The capillary voltage was set to 3.5 kV, cone voltage 25 V, source temperature 65 °C and desolvation temperature 100 °C. Nitrogen was used as the drying gas, at a flow rate of 320 L h^{-1}. In all collision induced dissociation (CID) scans, argon was used as the collision gas at a pressure of 3 mTorr, and the collision energy was 15–25 eV, depending on the fragility of the isolated ion.

TLC separation of analytes in irradiated samples was performed on 2.5 cm × 7.5 cm glass backed normal phase TLC plates (silica gel 60 F_{254}, Merck, Darmstadt, Germany). The plate was developed in a mobile phase of 1 : 1 ethyl acetate:hexane containing 1% (w/w) triethylamine. A basic permanganate staining solution was prepared by addition of $KMnO_4$ (1 g), K_2CO_3 (7 g), and NaOH (0.1 g) to water (100 cm^3). The developed plates were dipped into the permanganate solution and then completely dried using a heat gun.

Computational procedures

Standard *ab initio* molecular orbital theory and density functional theory calculations were carried out using Gaussian 09[19] and MOLPRO 2009.1.[20] Calculations were performed at a high level of theory, recently demonstrated to predict solution-phase bond dissociation energies and associated equilibrium constants to within chemical accuracy.[21] Geometries of all species were fully optimised at the B3-LYP/6-31G(d) level of theory. For all species, full systematic conformational searches (at a resolution of 120°) were carried out to ensure global, and not merely local, minima were located. Frequencies were also calculated at this level and scaled by recommended scale factors.[22] Improved energies for all species were calculated using the G3(MP2)-RAD level of theory, a high level composite *ab initio* method that approximates URCCSD(T) calculations with a large triple zeta basis set using additivity approximations.[23] This method was recently shown to reproduce a large test set of experimental gas-phase BDEs to within chemical accuracy.[24]

Entropies and thermal corrections were calculated using standard formulae[25] for the statistical thermodynamics of an ideal gas under the harmonic oscillator approximation in conjunction with the optimised geometries and scaled frequencies, and reaction

Gibbs free energies were computed using the Gibbs fundamental equation. Free energies of solvation were computed using the polarised continuum model, PCM-UAKS,[26] also at the B3-LYP/6-31G(d) level. Geometries of all species were re-optimised in solution. Free energies of each species in water solution at 298.15 K were calculated as the sum of the corresponding gas-phase free energy and the obtained free energy of solvation. The phase change correction term $RT(\ln V)$ was included in the energy of all species. Gibbs free energies of activation for the reactions involving a hydrogen transfer have been corrected for the effects of tunnelling using the standard formulae: $\Delta G^{\ddagger}_{corr} = \Delta G^{\ddagger} - RT\ln(\kappa(T))$, where $\kappa(T)$ is the tunnelling correction factor, T is the absolute temperature, R is the universal gas constant and $\Delta G^{\ddagger}$ is the Gibbs free energy of activation.[27]

Results and discussion

ESR characterisation of TEMPO derivatives

Initially, the ESR spectra of TEMPO **1** and derivatives containing at least one hydrogen at the 4-position (**2–4**) are characterised by fairly broad ESR lines as a result of the unresolved couplings to the methyl hydrogens.[28] In contrast, the spectrum of TEMPONE **5** shows much sharper lines with well resolved ^{13}C-coupling, due to the restrictions placed on the piperidine ring conformation by the ketone double bond.[29] Typical g-values and coupling constants are given in Table 1, and show good agreement with the available literature data.[30]

Reaction monitoring by ESR

While there is some debate about the exact role of free HO$^{\bullet}$ and surface charge carriers (photo-generated electrons and holes) in TiO_2 photocatalysis,[31] this approach provides mild conditions in which to monitor TEMPO oxidation. The conditions employed here were modelled on previous ESR experiments in which HO$^{\bullet}$ production was monitored by either spin-trapping,[32] or nitroxyl radical decay.[33] By using low concentrations of TiO_2 and the TEMPO derivatives (**1–5**), combined with a controlled irradiation regime to investigate purely photocatalytic reactions, extended periods of irradiation (up to 6 h) were possible without unwanted photochemical side reactions. Direct absorbance and subsequent destruction of the nitroxyl moiety by photons of wavelength below 320 nm was excluded by the use of the green glass filter, transmitting only photons of wavelength greater than 375 nm.[34] Under our conditions, no changes were observed in the spectrum when a standard solution of TEMPOL was maintained with TiO_2 in darkness, nor when irradiated in the absence of TiO_2.

Table 1 ESR properties of nitroxyl radicals **1–5** in water at 293 K. Microwave power 2.0 mW; modulation frequency 100 kHz; modulation amplitude 0.2 mT

	R[4]	g	a^{14}_N/mT
1	H	2.00563	1.73
2	OH	2.00570	1.71
3	OCH_3	2.00568	1.70
4	COOH	2.00566	1.71
5	=O	2.00562	1.61

ESR spectra are presented as a function of irradiation time for TEMPOL in Fig. 2. The initial spectrum is shown in Fig. 2(a). As the irradiation proceeds, asymmetry is observed after 30 min, indicative of a mixture of nitroxyl radicals. Distinctive features of a second radical begin to emerge after 70 min, particularly on the $M_I = -1$ line, as in Fig. 2(b). After 150 min, these features of the emerging radical become clear (Fig. 2c). The experiment continues until after 360 min the new radical is the only species present in the spectrum (Fig. 2d). Alongside Fig. 2(b) and 2(c), Fig. 2(e) and 2(f) are the spectra obtained by gradual addition of TEMPONE **5** to a solution of TEMPOL without irradiation. Fig. 2(g) is a spectrum of pure TEMPONE. These pairs of spectra confirm the nature of the radical mixture observed during the experiment to be TEMPOL and TEMPONE.

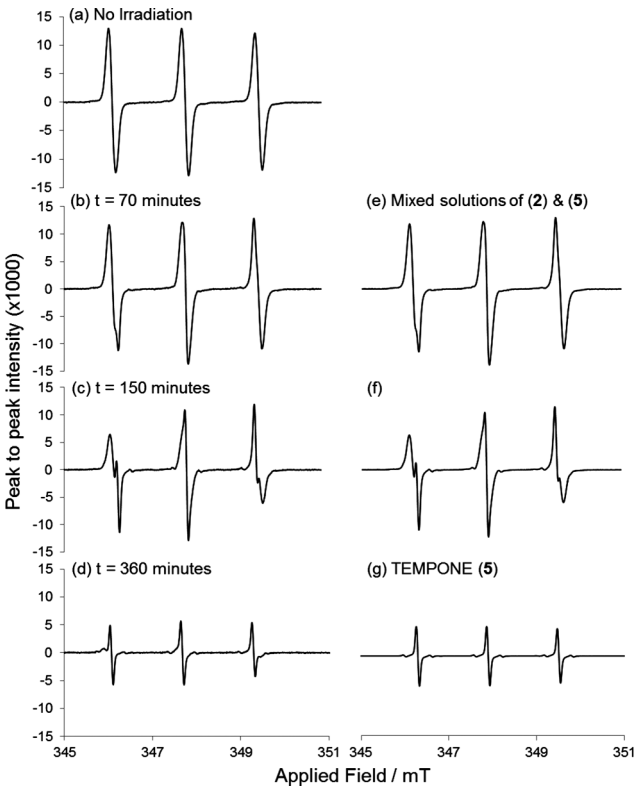

Fig. 2 ESR spectra of TEMPOL **2** as a function of irradiation time in the presence of P-25 TiO_2. (a) No Irradiation; (b) 70 min; (c) 150 min; (d) 360 min; (e), (f) dropwise addition of TEMPONE to TEMPOL to reproduce (b) and (c); (g) standard TEMPONE **5**.

This general pattern of results was repeated for the irradiation of both 4-methoxy-TEMPO **3** and 4-carboxy-TEMPO **4**, with the observed formation of TEMPONE concurrent with decreasing intensity of the parent nitroxyl radical. No other paramagnetic product species were identified. When either TEMPO **1** or TEMPONE **5** are exposed to the same conditions and subjected to the same analysis, no changes to the coupling constants are observed, the signal merely decays over time until no nitroxyl radicals are detectable after 3 h.

The total peak to peak signal intensity ($\Delta M_I = -1$ line) attributable to each of the TEMPO derivatives **2–4** as a function of time is plotted in Fig. 3, along with the formation of TEMPONE

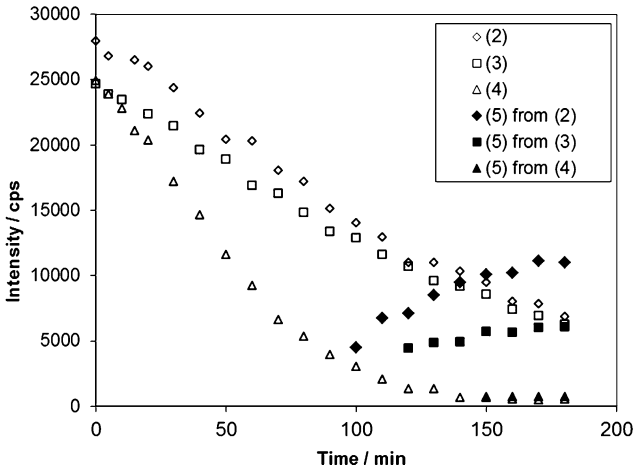

Fig. 3 Photocatalytic consumption of TEMPO derivatives **2–4** (open shapes) with the concurrent formation of TEMPONE **5** (filled shapes) as a function of irradiation time as detected by ESR.

5. For clarity, only the first 3 h of irradiation are shown. In all cases, the initial nitroxyl radical concentration is depleted (open shapes) and an increase in abundance of TEMPONE is observed (corresponding filled shapes). Data for the formation of TEMPONE are not present prior to 100 min, as the narrow peaks are obscured by the broader peaks of **2–4**. The rate at which the nitroxyl radical signal diminishes follows the trend of **4** > **3** > **2** and is thus clearly a function of the substituent in the 4-position of the piperidine ring (R^4 = CO_2H > OCH_3 > OH). This is broadly consistent with the trend in redox potentials of these nitroxyl radicals (*e.g.*, corrected E°(**4**) = 0.924 V *versus* E°(**2**) = 0.877 V)[35] and, in-line with previous studies, suggests that oxidation to the diamagnetic oxoammonium cation may be a major reaction pathway.[36]

The rate and abundance of TEMPONE **5** formation is similarly dependant on R^4, and does not form at all in the absence of a substituent in the 4-position, as demonstrated by the irradiation of TEMPO **1**. In every case, the yield of **5** is less than would be expected if all of the reactant had been transformed to this product, indicating that this is a minor pathway in the overall reaction scheme, while the bulk of the products are diamagnetic (see above). From the relative signal intensities of standard solutions of TEMPOL **2** and TEMPONE it can be estimated that TEMPONE formation from TEMPOL accounts for *ca*. 12% of the theoretical yield. Similarly, for 4-methoxy-TEMPO **3**, the formation of **5** is only *ca.* 6% of the theoretical yield, and for 4-carboxy-TEMPO **4** the yield is less than 1%. While TEMPONE formation in these instances is clearly a minor product, its observation is significant because only the hydroxyl radical driven conversion of TEMPOL to TEMPONE has previously been reported. Indeed, previous studies of HO$^\bullet$ reactivity with **4** did not report TEMPONE formation.[36] Overall the differing yields of TEMPONE from precursors **2–4** indicate that R^4 has a pronounced effect on the propensity for formation of this product. This observation is not correlated to the relative trend for the disappearance of the reactant (see above), perhaps unsurprisingly given that the latter is predominantly driven by modification of the nitroxyl moiety.

Table 2 Mass-to-charge ratio (*m*/*z*) and relative intensities (shown in parentheses and uncorrected for isotopic contributions) obtained from ESI-MS analysis of **1–5** in 4 : 1 CH_3CN : H_2O

	R^4	M^+	$[M+H]^{+\bullet}$	$[M+H_2]^+$	$[M-14]^+$
1	H	156.3 (13.0)	157.3 (84.5)	158.3 (56.6)	142.2 (100.0)
2	OH	172.3 (38.9)	173.3 (14.8)	174.3 (100.0)	158.2 (48.1)
3	OCH_3	186.3 (11.3)	187.3 (17.8)	188.4 (100.0)	172.3 (37.5)
4	COOH	200.3 (20.7)	201.3 (11.6)	202.3 (100.0)	186.3 (32.9)
5	=O	170.3 (16.3)	171.3 (16.8)	172.3 (100.0)	156.3 (45.0)

Characterisation of TEMPO derivatives by ESI-MS

ESI-MS analyses were undertaken to provide complementary detection of diamagnetic products arising from photocatalytic degradation of TEMPO derivatives **2–4**. It should be noted that under these conditions ESI-MS is not quantitative and cannot be used in this manner to provide a comprehensive mass-balance for the reaction. This is due to (i) the differences in ionisation efficiencies among the different species present (*e.g.*, Table 2) and (ii) the possibility that extensive oxidative fragmentation may result in low molecular weight products that can be volatilised from the reaction vessel. Despite these stated limitations, ESI-MS is a well recognised method for reaction monitoring, including those employing photocatalytic TiO_2,[37] and has proven particularly effective at identifying reaction intermediates.[38]

Prior to irradiation, the initial positive ion ESI mass spectra of the nitroxyl radicals display a distribution of ions around the molecular mass M. As redox processes can play a role in electrospray ionisation, the observation of multiple ions in the molecular ion region can be attributed to oxidation and reduction of the nitroxyl moiety under positive ion ESI conditions.[39] The M^+ oxoammonium cation, $[M+H]^{+\bullet}$ protonated nitroxyl radical cation, and $[M+H_2]^+$ protonated hydroxylamine cation are observed in varying abundances, with a strong dependence on the analyte, as well as the solvent and source conditions.[40] Typical abundances of these ions obtained from ESI-MS of **1–5** are provided in Table 2. Collision induced dissociation (CID) of these ions gave rise to fragmentation patterns similar to those obtained for larger *N*-ether HALS analogues previously reported.[41] For example, one prominent product ion observed in the CID of the $[M+H_2]^+$ ions is protonated acetone oxime $[(CH_3)_2C{=}NHOH]^+$, comprised of two hindering methyl groups and the piperidinyl nitrogen at *m*/*z* 74. This is illustrated for TEMPOL **2** in Fig. 4(a).

From Table 2 it is seen that an abundant ion, 14 Da below the molecular mass, is also observed in positive ion ESI-MS spectra of **1–5**. CID of the $[M-14]^+$ peak of TEMPOL **2** at *m*/*z* 158 is shown in Fig. 4(b), with the product ion at *m*/*z* 74 corresponding to protonated acetone oxime noticeably absent. Rather, fragmentation to an equivalent propan-2-iminium ion $[(CH_3)_2C{=}NH_2]^+$ is observed 16 Da lower at *m*/*z* 58 suggesting that the loss of 14 Da from the precursor nitroxyl radical results from reductive formation of $[M+H_2-O]^+$, rather than the isobaric $[M+H-CH_3]^{+\bullet}$ radical ion. Indeed, the CID spectrum shown in Fig. 4(b) is identical to that obtained from the $[M+H]^+$ ion of an authentic sample of 4-hydroxy-2,2,6,6-tetramethylpiperidine (denoted **2H**, data not shown). The presence of these piperidine ions at $[M-14]^+$ could be due to their presence in the samples themselves or they might arise during the ESI process. To assess these possibilities, the carboxylate functionality enabled

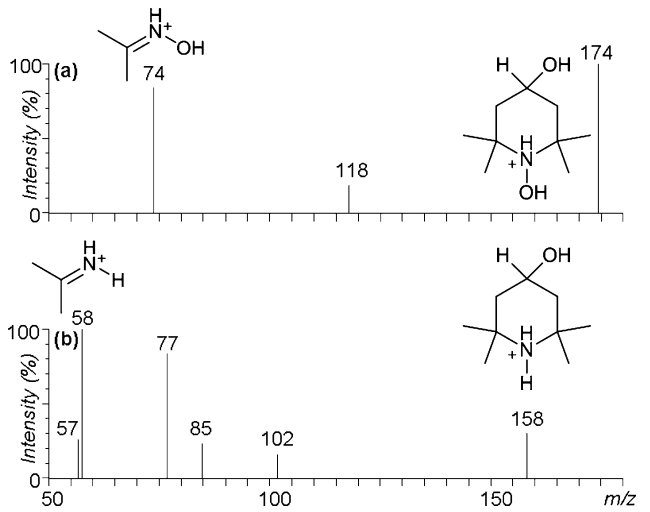

Fig. 4 CID mass spectra (obtained at a collision energy of 15 eV) of selected ions arising from ESI-MS analysis of TEMPOL **2** in 4 : 1 $CH_3CN : H_2O$. (a) $[M+H_2]^+$ at m/z 174 and (b) $[M+H_2–O]^+$ at m/z 158.

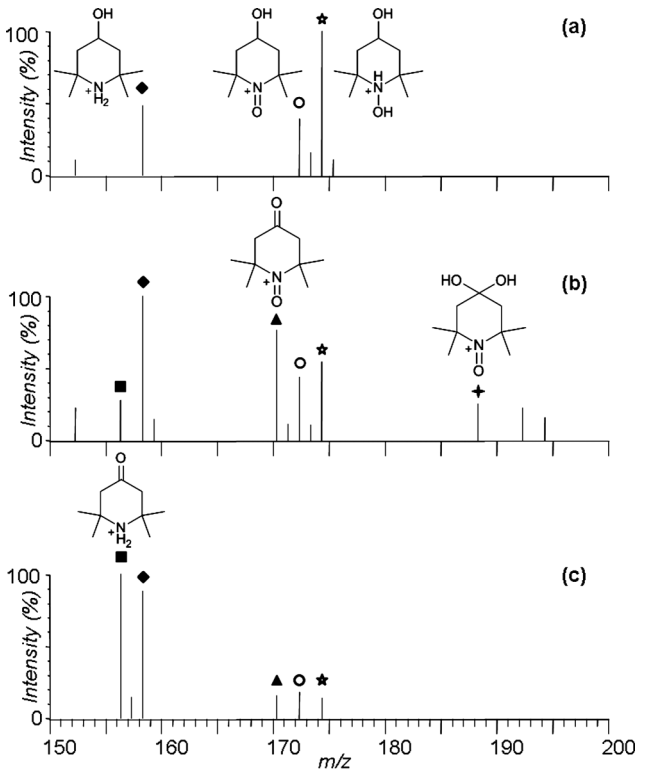

Fig. 5 ESI-MS spectra of **2** (in 4 : 1 $CH_3CN : H_2O$) at various stages of irradiation in the presence of TiO_2. Oxidation products TEMPONE **5**, and piperidines **2H** and **5H** are highlighted. (a) Pre-irradiation; (b) during irradiation; (c) post-irradiation.

4-carboxy-TEMPO **4** to also be detected as an $[M–H]^-$ ion in negative ion ESI. In this case, where the charge is maintained remote from the nitroxyl moiety, $[M–H]^-$ is the only peak observed in the molecular ion region at m/z 199, *i.e.*, no $[M–H–14]^-$ was observed. Furthermore, the $[M–14]^+$ peak can be eliminated from the positive ion spectra entirely by changing the solvent system from a mixture of acetonitrile and water to acidified methanol. Moreover, when the analytes **1–5** are developed by thin-layer chromatography, only one spot is observed, indicating that the additional $[M–14]^+$ peak is most likely a consequence of the modification of the nitroxyl moiety by positive ion ESI, rather than solution processes. ESI-MS and CID analyses of derivatives **3–5** exhibited similar results as described above for TEMPOL **2**. However, neither m/z 58 nor 74 are observed in the CID spectrum of **1** or **1H**, suggesting that this fragmentation process is dependent on R^4.

ESI-MS analysis of photo-oxidation products

Multiple studies have reported on the non-radical products arising from the reaction of TEMPO derivatives with $HO^•$ under different conditions. Oxidation of the nitroxyl moiety to the oxoammonium cation was reported as one product, while another study reported reduction of the nitroxyl to the hydroxylamine, where the nitroxyl was recovered upon addition of potassium ferricyanide.[16b,c] These species are indistinguishable from the nitroxyl radical in positive ion ESI-MS, as all three oxidation states of the nitroxyl are intrinsically present in the spectrum at M^+, $[M+H]^+$, and $[M+H_2]^+$ (Table 2). With this in mind, ESI-MS spectra were concurrently taken during the course of the irradiation to complement the ESR data and provide additional insight into the nature of the non-radical oxidation products of the TEMPO derivatives. Fig. 5 shows a series of ESI spectra of TEMPOL **2** when irradiated in the presence of TiO_2 over the same time course as the ESR analysis (Fig. 2). Consistent with ESR findings, no changes are observed in the spectrum when TEMPOL is irradiated with UV light in the absence of TiO_2, or when mixed with TiO_2 in darkness. At no stage are peaks attributable to dimers observed at multiples of the molecular mass.[13a,33]

The initial series of ions in Fig. 5(a) are consistent with those reported for TEMPOL **2** in Table 2. During (Fig. 5b) and following (Fig. 5c) irradiation, the M^+ and $[M+H_2]^+$ ions at m/z 172 and m/z 174 (open shapes) respectively, are diminished and predominantly supplanted by an ion at m/z 170, along with an ion at m/z 156 and an increase in the relative abundance of the ion at m/z 158 (filled shapes). The appearance of the ion at m/z 170 and its companion at m/z 156 would appear to be consistent with the formation of TEMPONE **5**, corroborating the ESR observations. The CID spectrum of m/z 170 however, is not an exact match with that obtained from the equivalent ion derived from ESI of an authentic sample of **5** (data not shown). This likely indicates the presence of a second, isobaric, product perhaps arising from dehydrogenation of the piperidine ring. Consistent with the ESR data, a putative TEMPONE ion at m/z 170 was also observed as a reaction product from **3** and **4** (ESI Fig. S1 & S2, respectively‡). In the absence of isobaric ions in both these cases the CID spectrum matches that of authentic **5**. Thus, on the basis of both ESR and ESI-MS observations, the formation of TEMPONE upon reaction with $HO^•$ is not limited to **2**. Rather, TEMPONE was detected following irradiation of any 4-substituted analogue **2–4**. In contrast, neither of the product ions at m/z 170 and m/z 156 are observed by ESI-MS during the irradiation of TEMPO **1** (data not shown), just as no ESR signal attributable to **5** is observed in these experiments. This supports the conclusion that where TEMPONE

formation is observed, the 4-substituent must be implicated in the reaction mechanism.

The $[M+16]^+$ ion, denoted by a solid cross at m/z 188 in Fig. 5(b), is observed during the oxidation of TEMPOL **2** and an analogous $[M+16]^+$ species is also observed for the reactions of **3** and **4** (ESI Fig. S1 & S2, respectively‡). These observations are consistent with a net increase of one oxygen atom of mass 16 Da. Multiple additions of oxygen at 16 Da intervals were not observed at any point. The CID spectra of the $[M+16]^+$ peaks exhibit characteristic losses of water (−18 Da) and R^4-H (*i.e.*, H_2O, CH_3OH or HCO_2H for **2**, **3** and **4**, respectively), indicating the presence of a hydroxyl moiety possibly the result of hydrogen abstraction followed by $HO^{\bullet}$ addition as previously proposed.[16b] While the position of the hydroxyl group is not certain, it is consistent with the 4,4-dihydroxylated species outlined in Scheme 2 for **2**, however analogous hydroxylation at other sites cannot be excluded. Indeed calculations of the barriers for hydrogen atom abstraction indicate a preference for initial radical formation and thus possible hydroxylation at the 3-position and perhaps even the methyl moieties (see below).

Although the $[M-14]^+$ ion at m/z 158 (Fig. 5, filled diamonds) was shown to form during positive ion ESI-MS of TEMPOL **2**, it is unexpectedly observed to increase in abundance upon irradiation in the presence of TiO_2 despite a concomitant decrease in other signature ions at m/z 172 and 174. Furthermore, when the irradiated solutions are analysed by TLC, a second spot is observed with a retention factor equal to the corresponding 4-hydroxy-2,2,6,6-tetramethylpiperidine **2H**, whereas only the nitroxyl spot is observed prior to irradiation. CID of the $[M-14]^+$ ions yield the same spectrum as pre-irradiation, indicating that **2H** remains present. This suggests that while the ion at m/z 158 in Fig. 5(a) arises exclusively from ionisation of TEMPOL **2**, two different sources contribute to this ion abundance in Fig. 5(b) and (c) and thus authentic **2H** is present in the irradiated solutions as an oxidation product. The contribution of the latter dominates in Fig. 5(c) and is consistent with ESR data suggesting a decreased concentration of TEMPOL **2**. Fig. 5 also reveals an increase in abundance of an ion at m/z 156 upon oxidation of TEMPOL under these conditions with this ion dominating the post-irradiation spectrum at the expense of TEMPONE at m/z 170 (Fig. 5c). The CID spectrum of m/z 156 that arises from the irradiation of TEMPOL **2** is shown in Fig. 6(a) and is identical to standard 4-oxo-2,2,6,6-tetramethylpiperidine **5H** (Fig. 6b). The presence of the characteristic iminium product ion at m/z 58 in both spectra confirms the presence of the secondary amine functionality in this ion. The formation of **5H** in these experiments appears to be a result of conversion of TEMPOL **2** to TEMPONE **5** with subsequent deoxygenation (as described below).

Increased abundances of equivalent $[M-14]^+$ ions are also observed during the irradiation of derivatives **3–5**, but the trend is most obvious for TEMPO **1**, because of the absence of the competing pathway for formation of TEMPONE **5**. Reduction of TEMPO **1** to the corresponding secondary amine **1H** is the predominant feature of the ESI spectrum, resulting in an abundant ion at m/z 142. Although $[M-14]^+$ ions are initially present in the mass spectra as a consequence of the ESI process, this combination of data infers that the 2,2,6,6-tetramethylpiperidines **1H–5H** are diamagnetic products arising from photo-oxidation of **1–5**, and

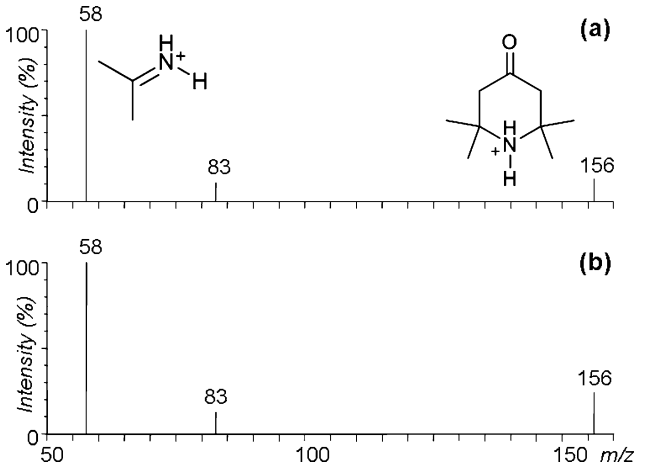

Fig. 6 CID mass spectra (obtained at a collision energy of 15 eV) of the ion at m/z 156 arising from ESI-MS analysis of: (a) a standard solution of 4-oxo-2,2,6,6-tetramethylpiperidine **5H**, and (b) irradiation of TEMPOL **2** in the presence of TiO_2.

moreover, that **5H** is observed at m/z 156 from each of **2–4**. This deoxygenation reaction is consistent with previous observations of the reduction of cyclic 5-membered nitroxyl radicals to amines when irradiated in the presence of TiO_2,[33] and the detection of hindered piperidines from active HALS in weathered polymer coatings.[42]

The formation of piperidines from *N*-oxyl piperidines **1–5** during photooxidation in the presence of TiO_2 could arise *via* one or all of the mechanisms outlined in Scheme 3. Combination of an alkyl radical ($R^{\bullet}$) with the nitroxyl oxygen results in an intermediate amino ether (Scheme 3a). Although the formation of aminyl radicals is often considered unlikely, for particular R groups it has been shown that cleavage of the N–OR bond is thermodynamically favoured over NO–R bond cleavage, releasing an aminyl radical rather than a nitroxyl.[21] The formed aminyl radical may then abstract an available hydrogen to form the secondary piperidine. Given the expected low concentration of suitable alkyl radicals under our experimental conditions this pathway is unlikely to dominate. Alternatively, addition of a peroxyl radical to the nitroxyl results in the formation of aminyl radical along with an alkoxyl radical and molecular oxygen

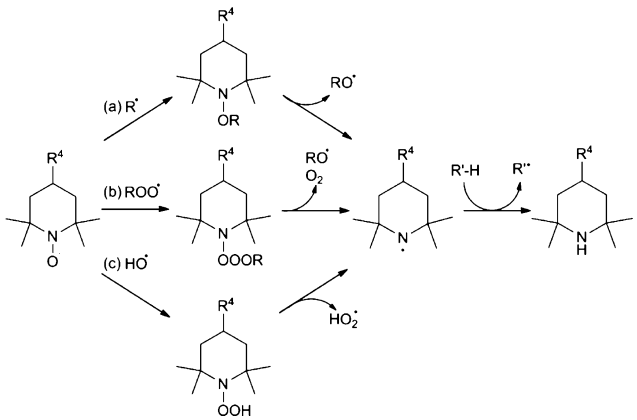

Scheme 3 Potential formation mechanisms of N–H piperidines from nitroxyl radicals by: (a) alkyl, (b) peroxyl, or (c) hydroxyl radical addition to TEMPO derivatives.

(Scheme 3b), however for the present species, the first step in this process is slightly endothermic (8.5 kJ mol^{-1}) and has a significant energy barrier (72 kJ mol^{-1}).[43] Similarly, addition of HO$^{\bullet}$ to the nitroxyl oxygen, with subsequent cleavage of the nitrogen–oxygen bond can result in formation of the secondary amine and release of the hydroperoxyl radical (Scheme 3c),[33] however our unpublished calculations indicate that the decomposition step in this process is also significantly endoergic (146.7 kJ mol^{-1} at 298 K). Further pathways might also be possible *via* the intermediary oxoammonium cations formed by electron transfer, but the precise mechanism of these is currently unclear.[44] Such pathways may be favoured in aqueous media due to the stabilisation of the charged species afforded by solvation.[43] While several mechanistic possibilities are suggested in the literature there is no definitive explanation for secondary amine formation.

Computational investigation into the effects of the 4-position substituent

The observed oxidative modification at the 4-position of **2–4** warranted further investigation. The influence of this substituent on the adjacent carbon–hydrogen (H^4) bond dissociation enthalpy (BDE)—a parameter related to the stability of the intermediate carbon-centred radical resulting from the initial hydrogen abstraction—was compared to the C–H BDEs of the methylene ring hydrogens (H^3) and the hindering methyl hydrogens (denoted CH_3). Calculations were undertaken using the G3(MP2)-RAD approach at 298.15 K and are presented in Table 3. Consideration of reaction temperature and bulk solvent does not appear to have any significant effect on the observed trends (see Table S1 in ESI‡). The data in Table 3 demonstrate that for the 4-substituted TEMPO derivatives **2–4**, the C–H^4 BDE is significantly lower than the C–H BDEs of either the 3-position or in the hindering methyl groups. Furthermore, the C–H^4 BDE in the substituted analogues **2–4** is significantly lower (by at least 16 kJ mol^{-1}) than that in the archetypal TEMPO **1** system indicating stabilisation of the carbon-centred radicals resulting from H^4-abstraction. In contrast, the BDEs of the hindering methyl group hydrogens are consistent with those of TEMPO and are not significantly influenced by variations in the remote R^4 substituent. Similarly, C–H^3 BDEs are constant, except in the case of TEMPONE **5** (*ca.* 35 kJ mol^{-1} lower than **1–4**) due to the stabilising effect afforded by the conjugation with the neighbouring C═O bond.

Considering hydroxyl (HO$^{\bullet}$) and hydroperoxyl radicals ($HO_2^{\bullet}$) are likely reactive species arising from aqueous TiO_2 photocatalysis, the relevant BDE(HO–H) = 493 kJ mol^{-1} and BDE(HOO–H) = 366 kJ mol^{-1} were calculated at the same level of theory and at 298.15 K. Both computed values are in agreement with literature values.[45] Comparison of these values with the data in Table 3 demonstrates that abstraction of hydrogens by HO$^{\bullet}$ will be exothermic from all positions (*i.e.*, H^4, H^3 or CH_3). By contrast, abstraction of all hydrogens in the experimental compounds by $HO_2^{\bullet}$ would be thermodynamically disfavoured, consistent with our recent study of $HO_2^{\bullet}$ abstractions in other organic compounds.[46] Although H^4 generally has a lower BDE than either H^3 or CH_3 in the TEMPO compounds studied, these thermodynamic differences alone do not provide an explanation for the reaction at the 4-position observed by ESR and ESI-MS analysis. Therefore, a study of the transition states of hydrogen abstraction by HO$^{\bullet}$ was undertaken, and the resulting gas-phase activation energies are displayed in Table 4. The corresponding solution-phase data follow the gas-phase trends and are provided in Table S2 of the ESI.‡

The gas phase activation Gibbs free energies of CH_3 hydrogen abstractions from **1** and **2** were calculated to be *ca.* 25 kJ mol^{-1}, and are assumed to be approximately constant with changes to the remote R^4 substituent in both **3** and **4**. H^3 abstraction barriers varied from *ca.* 24–30 kJ mol^{-1} and were consistently lower for the substituted derivatives **2–4** than the corresponding activation energies for abstractions of H^3 from TEMPO **1** itself (*ca.* 34 kJ mol^{-1}). Conversely, the adjacent functional group (R^4) does not significantly lower the activation barrier of H^4 abstraction relative to TEMPO **1** with a barrier of *ca.* 35–38 kJ mol^{-1} in all cases except that of **2**. Whilst **2** appears to be a significant outlier, it should be noted that for this reaction, standard transition state optimisations for H^4 abstraction led to geometries in which the attacking $^{\bullet}$OH instead interacts with the covalently bound 4-OH substituent. For this system, a series of constrained optimisations were performed. While the final "transition structure" contains a single imaginary frequency consistent with H^4 abstraction, we expect that the resulting structure is not fully optimised and the reported barrier is thus likely to be significantly overestimated. Even so, in contrast to the thermochemistry (Table 3), calculation of the activation barriers of hydrogen abstraction (Table 4) suggests a clear kinetic preference for abstraction at H^3 and CH_3 over H^4. The increasing abstraction barrier heights in the order CH_3 < H^3 < H^4 can be attributed to polar inductive effects overriding the thermodynamic preference for the formation of α-radicals and is consistent with previous computational and experimental observations of other systems.[47] Based on these calculations, it is plausible to conclude that the formation of TEMPONE **5** in the experiments described above does not arise from any preferential hydrogen abstraction at the 4-position. Indeed hydrogen abstraction at the 3-position

Table 3 Gas phase carbon–hydrogen BDEs for 4-substituted TEMPO species, calculated at 298.15 K by the G3(MP2)-RAD method

		BDE/kJ mol^{-1}		
	R^4	H^4	H^3	CH_3
1	H	412.4	412.1	422.5
2	OH	392.1	414.1	427.5
3	OCH_3	396.2	414.9	430.4
4	COOH	378.0	415.5	427.7
5	═O	—	377.9	428.0

Table 4 Gas phase activation barriers for hydroxyl radical-induced hydrogen abstraction from 4-substituted TEMPO species, calculated at 298.15 K by the G3(MP2)-RAD method

		Free energy barrier/kJ mol^{-1}		
	R^4	H^4	H^3	CH_3
1	H	37.4	33.6	24.9
2	OH	105.5[a]	30.7	26.0
3	OCH_3	38.5	25.0	—
4	COOH	35.3	23.9	—

[a] Approximate barrier only (see text for further details).

and from the methyl groups is kinetically preferred, though given the generally low barriers abstractions at all positions are likely to take place to some extent. In order to rationalise TEMPONE formation, plausible reactions following formation of the carbon-centred radicals were considered in further detail. Although we do not exclude the possibility of H^4 abstraction from TEMPOL **2** based on the reported barrier, an alternate mechanism to TEMPONE formation unique to TEMPOL *via* an alkoxyl radical is also considered below.

Under the conditions of the experiments described above hydroxyl radicals and dioxygen are both present, with the latter estimated to be more concentrated by at least an order of magnitude.[33] Addition of hydroxyl radical to carbon-centred radicals arising from H^4, H^3 or CH_3 hydrogen abstraction from the 4-substituted TEMPO derivatives **2–4** would give rise to an even-electron alcohol. These isomeric species are all plausible intermediates and/or products of this reaction and could contribute to the observation of $[M+16]^+$ ions upon ESI-MS analysis of the

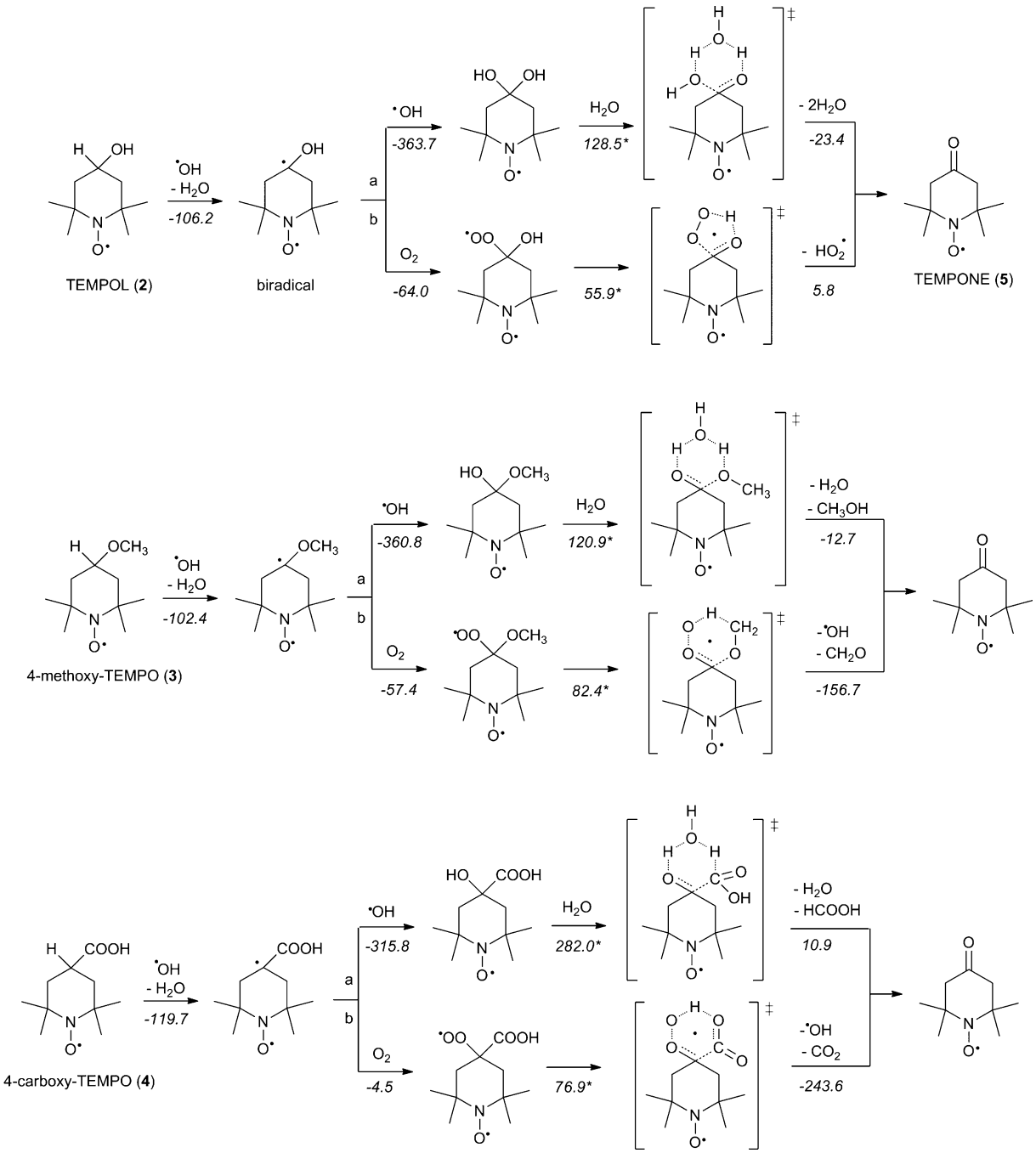

Scheme 4 After formation of a biradical by H^4 abstraction, (a) the product from recombination with HO$^\bullet$ can rearrange to TEMPONE through a 6-membered cyclic transition state with a water molecule to facilitate hydrogen transfer. (b) Alternatively, addition of O_2 to the biradical yields a peroxyl radical, which forms TEMPONE by intramolecular hydrogen transfer. Values in italics (in kJ mol^{-1}) correspond to gas-phase Gibbs free reaction energies and activation barriers (denoted by an asterisk).

reaction mixture (see above). Of these alcohols, only those arising from hydroxyl addition at the 4-position can reasonably give rise to formation of TEMPONE **5**. Calculations for reactions arising from the addition of HO$^{\bullet}$ to an alkyl radical centred on the 4-position have been undertaken and are summarised in Scheme 4(a). The corresponding solution-phase free energies follow the gas-phase results and are provided in Table S3 of the ESI.‡

These data indicate that the combination reaction of hydroxyl radical and HALS biradical is significantly exoergic, with free energies ranging from –316 kJ mol^{-1} for **4** to –364 kJ mol^{-1} for **2** relative to the nascent biradical in the gas phase. However, transition states for subsequent hydrolysis of the α-hydroxy intermediates to form TEMPONE were located and represent significant kinetic barriers to this reaction, ranging from 121 kJ mol^{-1} for **3** to 282 kJ mol^{-1} for **4**. While these barriers to direct hydrolysis mediated by a single water molecule may seem prohibitive, other pathways—especially those involving acid or base catalysis—may provide lower energy alternatives.

In contrast, addition of ground state molecular oxygen to the carbon centred radicals (Scheme 4(b)) was found to be mildly exoergic for **2** and **3** and negligibly exoergic for **4** due to the greater relative stability of the radical in the latter case (*cf*. Table 3). Significantly however, the barriers to unimolecular rearrangement of the peroxyl radicals to form TEMPONE were moderate in all cases, ranging from 56 kJ mol^{-1} for **2** to 82 kJ mol^{-1} for **3**. These calculations suggest that Scheme 4(b) provides a viable mechanism for the experimental observation of TEMPONE described above, consistent with previous proposals of carbonyl formation from α-hydroxy, α-methoxy, and α-carboxy peroxyl radical intermediates.[48] It should be noted however that O_2 addition to the intermediate biradicals is clearly reversible with the direct dissociation in the reverse direction entropically favoured over forward rearrangement to products. Therefore even with the greater abundance of O_2 compared to HO$^{\bullet}$ under the reaction conditions the irreversible trapping of the biradical as an alcohol is likely to be competitive, as evidenced by ESI-MS observations of $[M+16]^+$ ions.

For TEMPOL **2**, an alternative pathway to TEMPONE **5**, exclusive to this system, needs to be considered (Scheme 5). Abstraction of the hydrogen from the hydroxyl group itself would give rise to a nascent alkoxyl radical that could then donate a hydrogen atom to dioxygen (or another acceptor) to form the carboxyl moiety directly. Calculated kinetic and thermodynamic parameters (see also Table S3 in the ESI‡) are in favour of this pathway—both steps are exoergic and the activation barrier of hydrogen abstraction is plausible under the experimental conditions. Thus, **5** is likely to form from **2** *via* an alkoxyl radical rather than by thermodynamically reversible O_2 addition to an alkyl radical, a process which also involves a potentially prohibitive activation barrier to hydrogen abstraction. This alternate mechanism may also explain the higher yield for **5** arising from **2** compared to **3** or **4**, as observed by ESR (Fig. 3).

Conclusions

This work demonstrates the conversion of TEMPOL **2** to TEMPONE **5** from reaction with hydroxyl radicals generated by photocatalytic TiO_2 and further shows the broader applicability of this reaction to other 4-substituted TEMPO derivatives (**3**, **4**). Several putative mechanisms for the formation of TEMPONE initiated by hydrogen abstraction at the 4-position have been investigated by high level *ab initio* calculations and suggest both hydroxyl radical and dioxygen addition to the biradical intermediate may play a role in this conversion. A second TEMPONE formation mechanism unique to TEMPOL **2** *via* an alkoxyl radical was shown to be a plausible alternative to the peroxyl radical pathway. The quantitative loss of nitroxyl radicals observed by ESR during the oxidation (Fig. 3) can be rationalised by ESI-MS observations of formation of a secondary amine at the 1-position. This is broadly consistent with previous estimates of the sites of reaction in TEMPO derivatives that suggest *ca*. 40% of reactive encounters result in reaction at the nitroxyl moiety, with the remaining chemistry initiated by hydrogen atom abstraction at other sites.[44b] It is further consistent with our own observations of the conversion of functionalised HALS to the corresponding secondary amine in polymer coatings and detailed investigations of the mechanisms of this pathway and its consequences for the Denisov cycle (Scheme 1) are currently underway.[42b]

Experiments similar to those described herein with authentic HALS molecules are limited by their insolubility in aqueous media. It is not unreasonable however, to extend the current discussion to speculation of a plausible mechanism for HALS consumption in pigmented surface coatings, where TiO_2 is ubiquitously employed. Active HALS are recorded at highest concentrations in the top 30 μm of automotive clearcoats, near the air to polymer interface.[49] Coincidentally, this is the region of highest photocatalytic activity in TiO_2-pigmented materials,[50] given the necessity of moisture and oxygen to photocatalytic oxidation. It is plausible that a transient encounter between photocatalytically generated HO$^{\bullet}$ and a HALS molecule may lead to formation of TEMPONE by elimination of the HALS backbone (added for the very purpose of thermal stability). The active HALS moiety would subsequently be volatilised from the coating at service temperatures. Given that the elimination

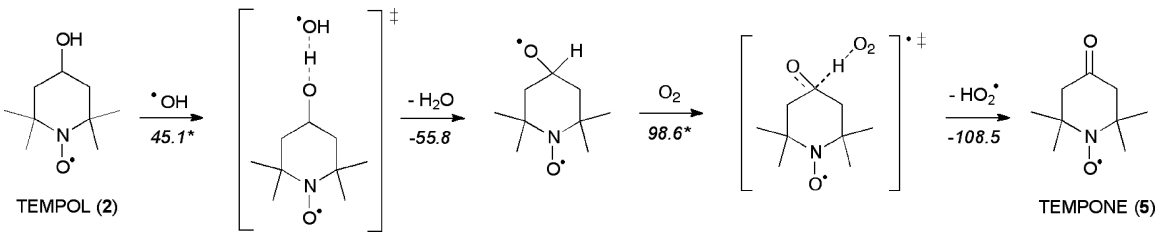

Scheme 5 Alternative pathway to TEMPONE **5** from TEMPOL **2** *via* an alkoxyl radical, which subsequently adds to O_2 and eliminates $HO_2^{\bullet}$. Values in italics (in kJ mol^{-1}) correspond to gas-phase Gibbs free reaction energies and activation barriers (denoted by an asterisk).

described herein is not the major pathway of HALS activity, and furthermore, that $HO^{\bullet}$ production is suppressed by TiO_2 surface modifications in durable pigments, the chances of these encounters would be low. However, over the entire lifetime of the polymer it may provide a significant, irreversible pathway for depletion of these otherwise demonstrably prophylactic additives.

Acknowledgements

We acknowledge the generous allocation of time on the National Facility of the National Computational Infrastructure in Canberra, Australia, which is supported by the Australian Commonwealth Government. S.J.B. and D.L.M. acknowledge funding from the Australian Research Council (ARC) and BlueScope Steel (LP0775032). S.J.B and M.L.Coote are funded through the ARC Centre of Excellence for Free Radical Chemistry and Biotechnology (CE0561607). D.L.M. is the holder of an Australian Postgraduate Award, and M.L.Coote acknowledges an ARC Future Fellowship.

References

1 R. G. Hicks, *Org. Biomol. Chem.*, 2007, **5**, 1321–1338.
2 (*a*) J. Chateauneuf, J. Lusztyk and K. U. Ingold, *J. Org. Chem.*, 1988, **53**, 1629–1632; (*b*) A. L. J. Beckwith, V. W. Bowry and K. U. Ingold, *J. Am. Chem. Soc.*, 1992, **114**, 4983–4992.
3 V. Chechik and G. Ionita, *Org. Biomol. Chem.*, 2006, **4**, 3505–3510.
4 (*a*) M. K. Georges, R. P. N. Veregin, P. M. Kazmaier and G. K. Hamer, *Macromolecules*, 1993, **26**, 2987–2988; (*b*) M. Conte, Y. Ma, C. Loyns, P. Price, D. Rippon and V. Chechik, *Org. Biomol. Chem.*, 2009, **7**, 2685–2687.
5 C. S. Wilcox and A. Pearlman, *Pharmacol. Rev.*, 2008, **60**, 418–469.
6 (*a*) F. Gugumus, in *Plastics Additives*, ed. R. Gächter and H. Müller, Carl Hanser Verlag, Munich, 4th edn, 1993, ch. 3, pp. 129–270; (*b*) C. Schaller, D. Rogez and A. Braig, *J. Coat. Technol. Res.*, 2009, **6**, 81–88.
7 (*a*) P. P. Klemchuk and M. E. Gande, *Polym. Degrad. Stab.*, 1988, **22**, 241–274; (*b*) F. Gugumus, *Polym. Degrad. Stab.*, 1993, **40**, 167–215; (*c*) E. N. Step, N. J. Turro, P. P. Klemchuk and M. E. Gande, *Angew. Makromol. Chem.*, 1995, **232**, 65–83.
8 (*a*) P. P. Klemchuk, M. E. Gande and E. Cordola, *Polym. Degrad. Stab.*, 1990, **27**, 65–74; (*b*) G. Geuskens and M. N. Kanda, *Polym. Degrad. Stab.*, 1996, **51**, 227–232; (*c*) O. Brede, D. Beckert, C. Windolph and H. A. Göttinger, *J. Phys. Chem. A*, 1998, **102**, 1457–1464; (*d*) I. Rossi, A. Venturini and A. Zedda, *J. Am. Chem. Soc.*, 1999, **121**, 7914–7917.
9 (*a*) F. Gugumus, *Polym. Degrad. Stab.*, 1995, **50**, 101; (*b*) J. L. Gerlock, C. A. Peters, A. V. Kucherov, T. Misovski, C. M. Seubert, R. O. Carter and M. E. Nichols, *J. Coat. Technol.*, 2003, **75**, 34.
10 (*a*) J. L. Gerlock, D. R. Bauer and L. M. Briggs, *Polym. Degrad. Stab.*, 1986, **14**, 53–71; (*b*) J. L. Gerlock, A. V. Kucherov and C. A. Smith, *Polym. Degrad. Stab.*, 2001, **73**, 201–210.
11 P. Yaneff, K. Adamsons, N. Cliff and M. Kanouni, *J. Coat. Technol. Res.*, 2004, **1**, 201–212.
12 G. Haacke, E. Longordo, F. F. Andrawes and B. H. Campbell, *Prog. Org. Coat.*, 1998, **34**, 75–83.
13 (*a*) K. Murayama and T. Yoshioka, *Bull. Chem. Soc. Jpn.*, 1969, **42**, 2307–2309; (*b*) G. Moad, E. Rizzardo and D. H. Solomon, *Tetrahedron Lett.*, 1981, **22**, 1165–1168; (*c*) G. S. Ananchenko and H. Fischer, *J. Polym. Sci., Part A: Polym. Chem.*, 2001, **39**, 3604–3621; (*d*) A. Nilsen and R. Braslau, *J. Polym. Sci., Part A: Polym. Chem.*, 2006, **44**, 697–717.
14 Y. Taguchi, Y. Ishida, H. Ohtani and H. Matsubara, *Anal. Chem.*, 2004, **76**, 697–703.
15 N. Haider and S. Karlsson, *Polym. Degrad. Stab.*, 2001, **74**, 103–112.
16 (*a*) U. Deffner and W. Schimmack, *Int. J. Radiat. Biol.*, 1976, **29**, 71–75; (*b*) K. Saito, J. I. Takeshita and T. Ozawa, *J. Pharm. Sci.*, 2003, **92**, 275–280; (*c*) W. Kudo, M. Yamato, K. Yamada, Y. Kinoshita, T. Shiba, T. Watanabe and H. Utsumi, *Free Radical Res.*, 2008, **42**, 505–512.
17 N. S. Allen, M. Edge, A. Ortega, G. Sandoval, C. M. Liauw, J. Verran, J. Stratton and R. B. McIntyre, *Polym. Degrad. Stab.*, 2004, **85**, 927–946.
18 P. J. Barker and A. Branch, *Prog. Org. Coat.*, 2008, **62**, 313–320.
19 M. J. Frisch, G. W. Trucks, H. B. Schlegel, G. E. Scuseria, M. A. Robb, J. R. Cheeseman, G. Scalmani, V. Barone, B. Mennucci, G. A. Petersson, H. Nakatsuji, M. Caricato, X. Li, H. P. Hratchian, A. F. Izmaylov, J. Bloino, G. Zheng, J. L. Sonnenberg, M. Hada, M. Ehara, K. Toyota, R. Fukuda, J. Hasegawa, M. Ishida, T. Nakajima, Y. Honda, O. Kitao, H. Nakai, T. Vreven, J. Montgomery, J. A., J. E. Peralta, F. Ogliaro, M. Bearpark, J. J. Heyd, E. Brothers, K. N. Kudin, V. N. Staroverov, R. Kobayashi, J. Normand, K. Raghavachari, A. Rendell, J. C. Burant, S. S. Iyengar, J. Tomasi, M. Cossi, N. Rega, N. J. Millam, M. Klene, J. E. Knox, J. B. Cross, V. Bakken, C. Adamo, J. Jaramillo, R. Gomperts, R. E. Stratmann, O. Yazyev, A. J. Austin, R. Cammi, C. Pomelli, J. W. Ochterski, R. L. Martin, K. Morokuma, V. G. Zakrzewski, G. A. Voth, P. Salvador, J. J. Dannenberg, S. Dapprich, A. D. Daniels, Ö. Farkas, J. B. Foresman, J. V. Ortiz, J. Cioslowski and D. J. Fox, *Gaussian 09, Revision A.02*, Wallingford, CT., 2009.
20 H.-J. Werner, P. J. Knowles, R. Lindh, F. R. Manby, M. Schütz, P. Celani, T. Korona, A. Mitrushenkov, G. Rauhut, T. B. Adler, R. D. Amos, A. Bernhardsson, A. Berning, D. L. Cooper, M. J. O. Deegan, A. J. Dobbyn, F. Eckert, E. Goll, C. Hampel, G. Hetzer, T. Hrenar, G. Knizia, C. Köppl, Y. Liu, A. W. Lloyd, R. A. Mata, A. J. May, S. J. McNicholas, W. Meyer, M. E. Mura, A. Nicklaß, P. Palmieri, K. Pflüger , R. Pitzer, M. Reiher, U. Schumann, H. Stoll, A. J. Stone, R. Tarroni, T. Thorsteinsson, M. Wang and A. Wolf, *MOLPRO 2009.1, a package of ab initio programs*, see http://www.molpro.net.
21 J. L. Hodgson, L. B. Roskop, M. S. Gordon, C. Y. Lin and M. L. Coote, *J. Phys. Chem. A*, 2010, **114**, 10458–10466.
22 A. P. Scott and L. Radom, *J. Phys. Chem.*, 1996, **100**, 16502–16513.
23 D. J. Henry, M. B. Sullivan and L. Radom, *J. Chem. Phys.*, 2003, **118**, 4849–4860.
24 M. L. Coote, C. Y. Lin, A. L. J. Beckwith and A. A. Zavitsas, *Phys. Chem. Chem. Phys.*, 2010, **12**, 9597–9610.
25 J. I. Steinfeld, J. S. Francisco and W. L. Hase, *Chemical Kinetics and Dynamics*, Prentice Hall, Englewood Cliffs, N.J., 1989.
26 J. Tomasi, B. Mennucci and R. Cammi, *Chem. Rev.*, 2005, **105**, 2999–3094.
27 M. L. Coote, *Macromol. Theory Simul.*, 2009, **18**, 388–400.
28 R. Chiarelli and A. Rassat, *Tetrahedron*, 1973, **29**, 3639–3647.
29 S. R. Burks, M. A. Makowsky, Z. A. Yaffe, C. Hoggle, P. Tsai, S. Muralidharan, M. K. Bowman, J. P. Y. Kao and G. M. Rosen, *J. Org. Chem.*, 2010, **75**, 4737–4741.
30 H. Fischer and K. H. Hellwege, ed., *Landolt-Börnstein: Numerical Data and Functional Relationships in Science & Technology*, Springer-Verlag, Berlin, 1979, vol. 9c.
31 (*a*) K. Ishibashi, A. Fujishima, T. Watanabe and K. Hashimoto, *J. Photochem. Photobiol., A*, 2000, **134**, 139–142; (*b*) Q. Xiang, J. Yu and P. K. Wong, *J. Colloid Interface Sci.*, 2011, **357**, 163–167.
32 M. A. Grela, M. E. J. Coronel and A. J. Colussi, *J. Phys. Chem.*, 1996, **100**, 16940–16946.
33 P. F. Schwarz, N. J. Turro, S. H. Bossman, A. M. Braun, A.-M. A. Abdel Wahab and H. Dürr, *J. Phys. Chem. B*, 1997, **101**, 7127–7134.
34 C. F. Chignell, A. G. Motten, R. H. Sik, C. E. Parker and K. Reszka, *Photochem. Photobiol.*, 1994, **59**, 5–11.
35 J. P. Blinco, J. L. Hodgson, B. J. Morrow, J. R. Walker, G. D. Will, M. L. Coote and S. E. Bottle, *J. Org. Chem.*, 2008, **73**, 6763–6771.
36 K. Takeshita, K. Saito, J.-i. Ueda, K. Anzai and T. Ozawa, *Biochim. Biophys. Acta, Gen. Subj.*, 2002, **1573**, 156–164.
37 R. M. Alberici, M. A. Mendes, W. F. Jardim and M. N. Eberlin, *J. Am. Soc. Mass Spectrom.*, 1998, **9**, 1321–1327.
38 L. S. Santos, ed., *Reactive Intermediates: MS Investigations in Solution*, Wiley-VCH, Weinheim, 2010.
39 (*a*) J. L. Hodgson, M. Namazian, S. E. Bottle and M. L. Coote, *J. Phys. Chem. A*, 2007, **111**, 13595–13605; (*b*) S. Manda, I. Nakanishi, K. Ohkubo, H. Yakumaru, K. I. Matsumoto, T. Ozawa, N. Ikota, S. Fukuzumi and K. Anzai, *Org. Biomol. Chem.*, 2007, **5**, 3951–3955.
40 (*a*) J. O. Metzger and J. Griep-Raming, *Eur. J. Mass Spectrom.*, 1999, **5**, 157–163; (*b*) C. D. Smith, J. P. Bartley, S. E. Bottle, A. S. Micallef and D. A. Reid, *J. Mass Spectrom.*, 2000, **35**, 607–611.
41 T. A. Lowe, M. R. L. Paine, D. L. Marshall, L. A. Hick, J. A. Boge, P. J. Barker and S. J. Blanksby, *J. Mass Spectrom.*, 2010, **45**, 486–495.
42 (*a*) J. L. Gerlock, T. Riley and D. R. Bauer, *Polym. Degrad. Stab.*, 1986, **14**, 73–84; (*b*) M. R. L. Paine, P. J. Barker and S. J. Blanksby, *Analyst*, 2011, **136**, 904–912.
43 J. L. Hodgson and M. L. Coote, *Macromolecules*, 2010, **43**, 4573–4583.
44 (*a*) R. L. Willson, *Int. J. Radiat. Biol.*, 1972, **21**, 401–403; (*b*) S. Goldstein and A. Samuni, *J. Phys. Chem. A*, 2007, **111**, 1066–1072.

45 S. J. Blanksby and G. B. Ellison, *Acc. Chem. Res.*, 2003, **36**, 255–263.
46 G. Gryn'ova, J. L. Hodgson and M. L. Coote, *Org. Biomol. Chem.*, 2011, **9**, 480–490.
47 (*a*) A. Samuni, S. Goldstein, A. Russo, J. B. Mitchell, M. C. Krishna and P. Neta, *J. Am. Chem. Soc.*, 2002, **124**, 8719–8724; (*b*) K. D. Beare and M. L. Coote, *J. Phys. Chem. A*, 2004, **108**, 7211–7221; (*c*) Z. I. Watts and C. J. Easton, *J. Am. Chem. Soc.*, 2009, **131**, 11323–11325.
48 (*a*) E. Bothe, M. N. Schuchmann, D. Schulte-Frohlinde and C. von Sonntag, *Photochem. Photobiol.*, 1978, **28**, 639–644; (*b*) R. Atkinson, *Chem. Rev.*, 1986, **86**, 69–201; (*c*) P. Ulanski, E. Bothe, K. Hildenbrand, J. M. Rosiak and C. von Sonntag, *J. Chem. Soc., Perkin Trans. 2*, 1996, 23–28; (*d*) E. M. Collins, H. W. Sidebottom, J. C. Wenger, S. Le Calvé, A. Mellouki, G. LeBras, E. Villenave and K. Wirtz, *J. Photochem. Photobiol., A*, 2005, **176**, 86–97.
49 J. L. Gerlock, A. V. Kucherov and M. E. Nichols, *J. Coat. Technol.*, 2001, **73**, 45–54.
50 H. G. Völz, G. Kämpf, H. G. Fitzky and A. Klaeren, *ACS Symp. Ser.*, 1981, **156**, 163–182.